Nanoscale

Accepted Manuscript

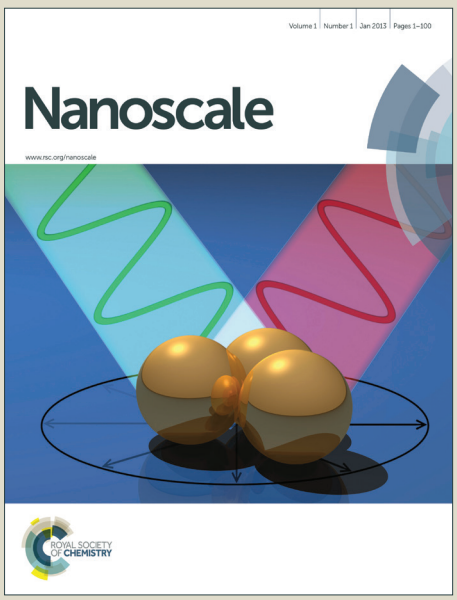

ROYAL SOCIETY OF CHEMISTRY

www.rsc.org/nanoscale

Journal Name

RSCPublishing

COMMUNICATION

Surface Al Leached Ti_3AlC_2 Substituting Carbon for Catalyst Support Served in a Harsh Corrosive Electrochemical System

Cite this: DOI: 10.1039/x0xx00000x

Received ooth January 2012,
Accepted ooth January 2012

DOI: 10.1039/x0xx00000x

www.rsc.org/

Xiaohong Xie, Yun Xue, Li Li,* Siguo Chen, Yao Nie, Wei Ding and Zidong Wei*

Surface Al leached Ti_3AlC_2 particles (e-TAC) with high corrosion resistance and excellent electrical conductivity were developed as an advanced support material for Pt catalyst. Electrochemical measurements confirm that the supported Pt/e-TAC electrocatalyst shows much improved activity and enhanced durability toward oxygen reduction reaction when compared with the commercial Pt/C catalyst.

Pt-based catalyst is one of the few catalysts that can work without much worry about durability in a harsh corrosive electrochemical system, such as the oxygen reduction reaction (ORR) in polymer electrolyte membrane fuel cells (PEMFCs).[1] Up to now, Pt/C catalyst with highly dispersed Pt nanoparticles (NPs, 2-5 nm) supported on carbon is still being widely used as the state-of-the-art commercial catalysts. However, the durability of the Pt/C catalyst is not satisfactory in PEMFCs.[2-3] The predominance of weak interactions between the carbon and the catalytic Pt NPs leads to aggregation of the Pt NPs and a consequent decrease in the Pt electrochemical surface area (ECSA) with long-term operation. More importantly, the carbon support is susceptible to corrosion because of the operating conditions of PEMFCs, which include high acidity, potential, humidity, and temperature (80 °C). The degradation of the Pt/C cathode catalyst induced by the carbon support is considered to be the main reason for the reduction of the catalytic activity and stability.[4]

Using a more stable carbon material, such as carbon nanotubes, graphene nanosheets, or carbon nanofibers, would alleviate the problems caused by the carbon support.[5-7] However, until now, none of the above carbon materials investigated were able to adequately prevent the electrochemical corrosion of carbon during extended operation and repeated cycling. Therefore, more robust and corrosion-resistant support materials should be developed. Recently, several titanium-based composite support materials (e.g., TiO_2, MWCNTs-TiO_2, and $Ti_{0.7}Ru_{0.3}O_2$) as alternatives to carbon have shown reduced ECSA degradation rates and improved stability.[8-10] However, the innate low conductivity of these titanium-based materials prevents their use in an electrochemical device, where electrons are either reactants or products; therefore, good electrical conductance is absolutely required.

The conducting titanium-and-carbon-rich Ti_3AlC_2, which is from a large family of layered hexagonal ternary metal carbides referred to as the MAX phase, has recently received our special attention for use as a promising support in Pt catalysts because of its high chemical stability and good electrical conductivity.[11] Nevertheless, nanosized Ti_3AlC_2 lacks sufficient binding sites to anchor the Pt precursors or Pt NPs due to its low surface area and the chemical inertness of the material surface, which may lead to poor Pt dispersion and large Pt NPs. To solve these problems and to make Ti_3AlC_2 a more efficient support, the incorporation of functional groups onto the Ti_3AlC_2 particles to modify its physicochemical properties and surface structure are necessary. Limited literature was found describing the modification of the Ti_3AlC_2 structure and the use of the corresponding products as catalyst supports.

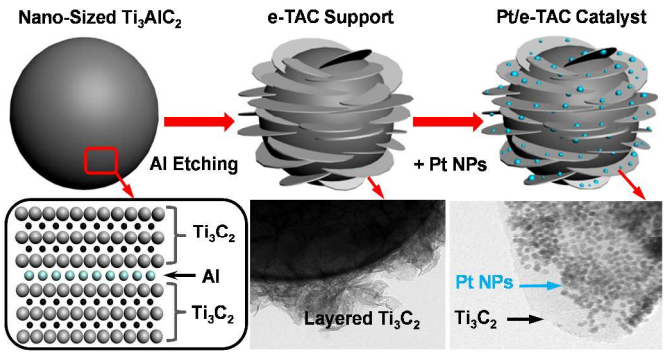

Scheme 1 Schematic of Pt/e-TAC catalyst formation

The present study highlights the development of a well-structured and well-functionalized Ti_3AlC_2 support material using an optimized hydrothermal etching method (Scheme 1). The newly developed method for modifying the pristine Ti_3AlC_2 material is environmentally friendly and simple.[12-13] More specifically, the developed fluoride-free method is more conducive to improving the corrosion resistance of the developed titanium-based materials, which has been proven to be unstable in a solution containing fluoride groups or ions.[14] The preparation procedures include the surface treatment of bulk Ti_3AlC_2 in an aqueous NaOH solution

followed by a H_2SO_4 hydrothermal treatment (See the Supporting Information). This strategy results in the selective leaching of Al layers in the layered Ti_3AlC_2 and the formation of surface exfoliated and OH-group-terminated Ti_3C_2 layers. The newly developed support material (surface Al etched Ti_3AlC_2, denoted as e-TAC) were then loaded with Pt NPs and tested as a catalyst (Pt/e-TAC) for the ORR. Interestingly, the use of e-TAC to support Pt NPs can overcome the above-mentioned disadvantages associated with carbon and low conductive Ti-based composites. That is, the high chemical stability can inhibit the corrosion of the support material, and the good electrical conductivity can effectively provide the electron transport pathway. The strong Pt interaction with e-TAC leads to highly dispersed and well-anchored Pt NPs. More specifically, the surface Ti_3C_2 layer structure of the e-TAC support acts as a co-catalyst for Pt, based on "electronic transfer mechanisms" from e-TAC support to Pt; that is, the shift in the d-band structure of the Pt NPs leads to weak interactions between Pt and the intermediate species, which is normally played by the second metal in the conventional Pt-M system, thereby, promoting the reduction of oxygen in a manner that a simple carbon support cannot.[15-18] Therefore, the newly developed Pt/e-TAC catalysts can outperform the most widely used commercial Pt/C catalyst in both activity and stability.

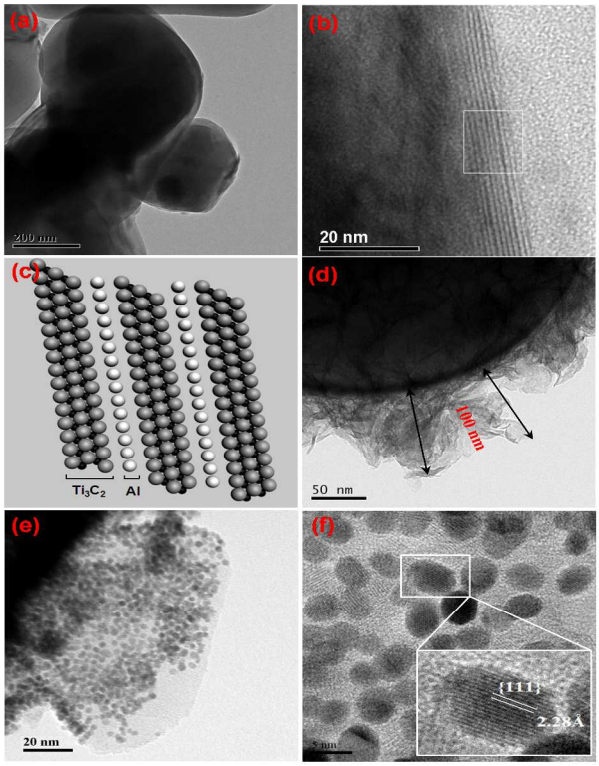

Fig. 1 TEM images of (a) pristine bulk Ti_3AlC_2, (b) HRTEM image of Ti_3AlC_2 laminated structure, (c) atom arrangement of square M in (b), (d) e-TAC material, (e) Pt/e-TAC catalyst, and (f) HRTEM of Pt/e-TAC.

The structures of the pristine Ti_3AlC_2 and of the prepared e-TAC support and Pt/e-TAC catalyst were determined using X-ray diffraction (XRD) measurements. Fig. S1 shows well-resolved diffraction peaks at 2θ values of 9.4°, 19.0°, 34.9°, 38.9° and 41.7°, which correspond to the characteristic peaks of pure hexagonal Ti_3AlC_2 crystal phases. Interestingly, after the loading of Pt NPs, the prepared Pt/e-TAC material exhibited an almost identical diffraction pattern as the original Ti_3AlC_2, with the exception of three Pt peaks: Pt(111), Pt(200) and Pt(220). This result indicates that etching of the Al atoms is mostly limited to the surface level of the particles even though the samples are dispersed in a NaOH solution for a prolonged period of time (100 h), which is attributed to the ultra-high chemical stability of Ti_3AlC_2 and the poor etching ability of the NaOH solution compared with the previously used HF solution.[13] This finding is also supported by the transmission electron microscopy (TEM) images of pristine Ti_3AlC_2 and the e-TAC (Fig. 1, Fig S2 and Fig. S3). Fig. 1a shows the morphology of the Ti_3AlC_2. Its laminated structure is also clearly displayed in Fig. 1b and schematically illustrated in Fig. 1c. Fig. 1d displays a special surface-modified structure of the e-TAC that is pertinent to this work and the thickness of the modification film is measured to be about 100 nm. The cicada wing-like Ti_3C_2 is grown on the bulk Ti_3AlC_2 with leaching of Al layers. This result also implies that the Ti_3C_2 layer is more chemically stable than Ti_3AlC_2 in both acidic and oxidizing environments. The X-ray photoelectron spectra (XPS) reveal that the surface elements of e-TAC contain more Ti and C but less Al than pristine Ti_3AlC_2 (Fig. S4), thus confirming the leaching of Al atoms and the formation of a Ti_3C_2 surface layer.

The nitrogen sorption (adsorption and desorption) isotherm and its corresponding BJH pore size distribution for the new e-TAC support material are shown in Fig. S5. The e-TAC exhibits a typical type IV isotherm with a distinct hysteretic loop (Fig. S 5a) attributable to the presence of the mesoporous structure in the e-TAC; this deduction is supported by the pore size distribution curve (Fig. S 5b), which shows that the pore size centre is approximately 1.8 nm for e-TAC. In addition, the BET surface area of the e-TAC (10.35 $m^2 g^{-1)}$ is approximately 10 times higher than that of pristine Ti_3AlC_2 (1.18 $m^2 g^{-1}$), as shown in Fig. S5, further confirmed the successful surface modification. The electrical conductivity of the e-TAC was measured to be approximately 4.3×10^{-2} S cm^{-1} (Fig. 2), which is comparable to carbon black (2.4×10^{-1} S cm^{-1}), but the value is significantly higher than the conductivity of commercial TiO_2.[19-20] The excellent conductivity of the e-TAC makes it a promising catalyst support for use in an electrochemical system.

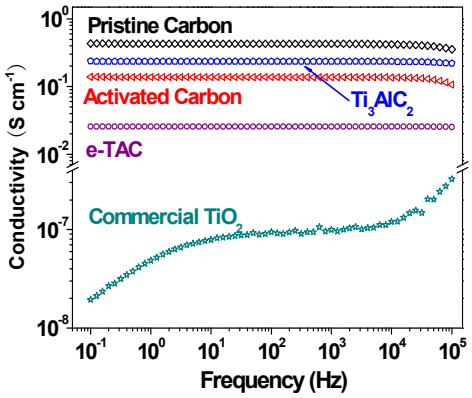

Fig. 2 Electrical conductivity of pristine carbon, activated carbon, commercial TiO_2, pristine Ti_3AlC_2 and the e-TAC support.

Upon deposition of the Pt, TEM images of the product Pt/e-TAC revealed that highly dispersed Pt NPs uniformly cover the Ti_3C_2 layer of the e-TAC (Fig. 1e); these small, well-dispersed Pt NPs have a very narrow size distribution between 2 and 5 nm. In addition, the HRTEM image of Pt/e-TAC (Fig. 1f) shows that the Pt NPs are tightly adhered to the Ti_3C_2 surface and revealed continuous lattice fringes from the Ti_3C_2 substrates to the supported Pt particles.

This result indicates that the Pt was grown epitaxially on the Ti_3C_2 surface. SEM-EDS (Fig. S6) applied directly to the Pt/e-TAC showed the presence of approximately 14.82 wt% Pt on e-TAC, which is consistent with the designed Pt content of 15 wt% in the catalyst preparation. The SEM-EDS also confirms the coexistence of Ti, Al, C, and Pt in the Pt/e-TAC catalyst, and these elements were uniformly distributed in the randomly selected area.

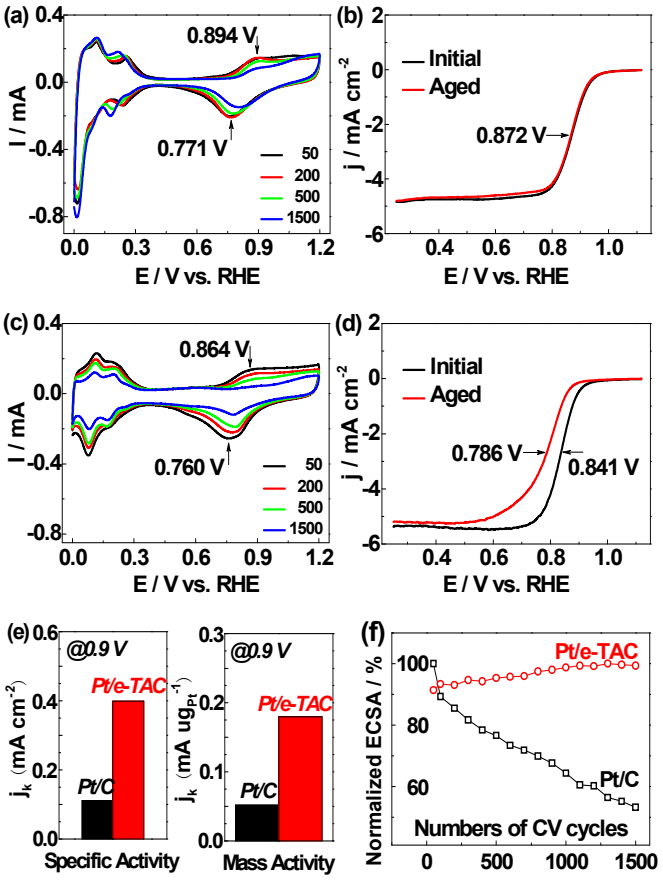

Fig. 3 CV curves for (a) Pt/e-TAC and (c) Pt/C catalysts (recorded in 0.1 M N_2-saturated $HClO_4$ with a scan rate of 50 mV·S^{-1}) and ORR polarization curves for (b) Pt/e-TAC and (d) Pt/C catalysts before and after the ADT cycling (recorded in O_2-saturated 0.1 M $HClO_4$ at 1600 rpm and with a scan rate of 10 mV·S^{-1}). (e) Specific activity and mass activity at 0.9 V for Pt/e-TAC and Pt/C catalysts. (f) Normalized Pt ECSA of Pt/e-TAC and Pt/C catalysts as a function of the number of CV cycles. Pt loading for both electrodes is about 10 ug.

The catalytic properties of Pt/e-TAC were studied and compared with the Pt/C (40 wt% Pt supported on Vulcan XC-72, JM) catalyst (Fig. 3). Fig. 3a and 3c show a subset of the cyclic voltammogram (CVs) curves for the two catalysts, which were recorded at room temperature in a N_2-purged 0.1 M $HClO_4$ solution at a scan rate of 50 mV s^{-1}. The CVs exhibited two distinct potential regions associated with H_{upd} adsorption/desorption processes between $0 < E < 0.3$ V and the formation of an OH_{ad} layer beyond 0.6 V, where the H_{upd} and OH_{ad} refer to underpotential-deposited hydrogen and adsorbed hydroxyl species, respectively. The ECSA was calculated by integrating the double layer corrected H_{upd} charge in the cathodic scan and dividing by the value of 210 uC cm^{-2} assumed for the adsorption of a hydrogen monolayer on polycrystalline Pt. The initial specific ECSA based on the Pt mass for Pt/e-TAC was estimated to be 44.81 m^2 g^{-1} (Fig. 3a, black curve), which was found to be similar to the Pt/C catalyst (47.05 m^2 g^{-1}, Fig. 3c, black curve).

Rotation-rate-dependent current density-potential curves of the Pt/e-TAC and Pt/C catalysts are given in Fig. 4. High rotational speeds result in the increase of oxygen diffusion to the electrode surface and remarkable reduction current density. The resulted Koutecky-Levich (KL) plots (j^{-1} vs. $\omega^{-1/2}$) for Pt/e-TAC at different potentials show good linearity and near parallelism of the fitting lines, indicating the first order kinetics with respect to dissolved O_2 and similar electron transfer numbers for ORR at different potentials. The electron transfer number (n) was calculated to be 3.9 for the Pt/e-TAC from the slopes of KL plots, which is consistent with the theoretical value for the ORR involving four-electron transfer. Polarization curves for the ORR on the catalysts are shown in Fig. 3b and 3d for Pt/e-TAC and Pt/C, respectively. The initial half-wave potentials for Pt/e-TAC and Pt/C were measured to be 0.872 V (Fig. 3b and Fig S 7a) and 0.841 V (Fig. 3d and Fig S 7b), respectively, which indicates that the Pt/e-TAC is more active for the ORR than Pt/C. As shown in Fig. 2e, the specific activity of the Pt/e-TAC is 0.399 mA cm^{-2} at 0.9 V, which is 3 times greater than that of Pt/C catalyst (0.111 mA cm^{-2}).[21] Similarly, after normalization to the loading amount of Pt metal (10 ug), the mass activity of the Pt/e-TAC (0.180 A mg_{Pt}^{-1}) is also 3 times greater than that of Pt/C (0.0518 A mg_{Pt}^{-1}).

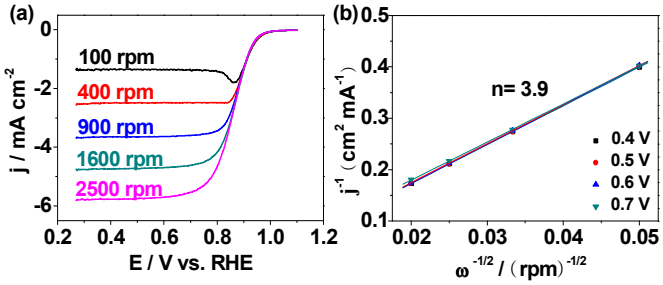

Fig. 4 (a) Room temperature rotating disk voltammograms of Pt/e-TAC electrocatalyst in O_2-saturated 0.1 M $HClO_4$. Sweep rate, 10 mV s^{-1}. (b) Corresponding Koutecky-Levich plots (j^{-1} vs. $\omega^{-1/2}$) at different potentials.

The electrochemical stability of Pt/TAC and Pt/C catalysts were evaluated by accelerated durability tests (ADT). Fig. 3a and 3c demonstrate that a considerable ECSA loss (approximately 48%) was observed for the Pt/C catalyst after 1,500 cycles. Whereas in the case of Pt/e-TAC, it is important to highlight that the normalized ECSA of Pt/e-TAC kept increasing slightly during the ADT cycling (Fig. 3f), which probably caused by the restructuring of the catalyst surface, indicating that the stability of the Pt/e-TAC is far superior to that of Pt/C.[22] Meanwhile, the catalytic activity of the Pt/e-TAC, assessed by the half-wave potential, showed no significant decrease after the ADT (Fig. 3b, red curve), while the activity decrease for Pt/C is 45 mV (Fig. 3d, red curve), indicating that the Pt/e-TAC catalyst is not only more stable but also more active than the Pt/C catalyst.

The morphologies of the Pt/C and Pt/e-TAC catalysts after the ADT are shown in Fig. 5. On the basis of the TEM results, the size distribution of the Pt particles is also calculated. For Pt/e-TAC, no noticeable ripening or aggregation of the Pt NPs is observed after 1500 CV cycles. The average size of the Pt NPs only slightly increased (Fig. 5a and 5b), which suggested that the Pt NPs were

tightly anchored and stabilized on the Ti_3C_2 layered structure of the novel e-TAC support. The considerably enhanced ORR stability of the Pt/e-TAC may be arise from the strong metal-support interaction between the Pt NPs and the e-TAC support, which prevents migration of the Pt NPs on the e-TAC support. In contrast, the average sizes of the Pt NPs in the Pt/C catalyst substantially increased from 2-5 nm to 3-17 nm with a broad size distribution (Fig. 5c and 5d), which confirms that the major cause of Pt/C degradation is the ripening or aggregating along with dissolution of Pt NPs due to poor binding between the Pt NPs and the carbon support.

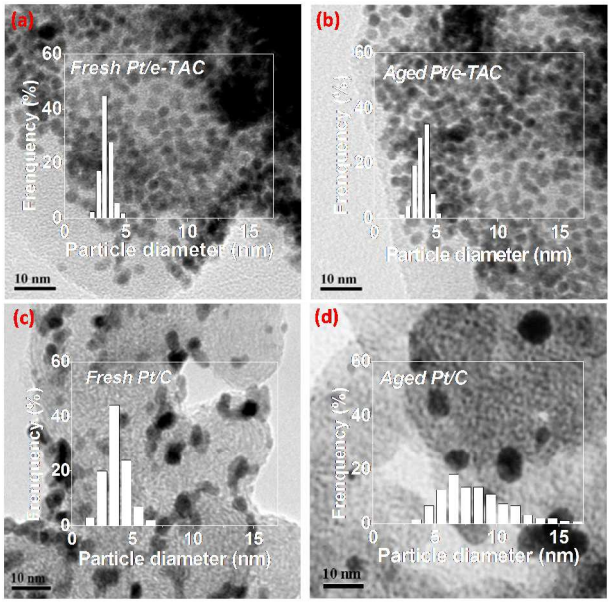

Fig. 5 TEM images of (a) fresh Pt/e-TAC catalyst, (b) aged Pt/e-TAC, (c) fresh Pt/C catalyst and (d) aged Pt/C. Inserted are Pt particle size distribution histograms.

Surface elemental composition analysis from XPS surveys of Pt/C and Pt/e-TAC catalysts before and after the ADT cycling (Fig. S8) also provided compelling evidence that the e-TAC support is more stable than carbon. The corresponding results are listed in Table S1. For the Pt/C catalyst, a significant decrease in the amount of surface carbon and an increase in the Pt content was observed after the ADT cycling. The loss of carbon from the Pt/C catalyst is attributed to the oxidation of carbon to CO or CO_2. This result further confirms that the electrochemical corrosion of the carbon support is one of the most critical issues affecting the long-term stability of the Pt/C catalyst. In a contrast to the dramatic loss of carbon content in the Pt/C catalyst, the Pt/e-TAC showed only a slight change in the surface element compositions, which illustrates that the composition of exfoliated Ti_3AlC_2, that is, e-TAC, almost remains the same before and after the ADT. In other words, e-TAC is stable enough to endure the harsh corrosive environment.

To further understand the excellent binding ability of Pt NPs on the e-TAC support (Ti_3C_2 layered structure) in comparison with that on the carbon support, DFT calculations were conducted (see Supporting Information for details). A Pt_{13} cluster was chosen on purpose for simulations of the Pt NPs due to the "magic number" 13 that provides a higher geometric and electronic stability than other clusters.[23] The optimized most stable structure of Pt_{13} loaded on the Ti_3C_2 and C are shown in Fig. 6a. The calculated binding energies (E_{bind}) of the Pt_{13} cluster is 5.499 eV on Ti_3C_2 but 3.362 eV on C, indicating a stronger interaction between Pt_{13} and the Ti_3C_2 compared to that between Pt_{13} on C. In Fig. 6, the partial density of state (PDOS) of Pt/Ti_3C_2 and Pt/C before and after adsorption also indicates that there is a strong interaction between Pt and Ti_3C_2. As revealed in Fig. 6b, there is a more considerable overlap near the Fermi level between the Pt-d states and the Ti-d states. The large overlap and a suitable energy match mean easier electron transfer between these states and the formation of the Pt-Ti bond. The formation of Pt-Ti bond is evidenced by the Pt-d states and the Ti-d states shifting to a lower energy, a more significant change relative to their free states prior to adsorption. Meanwhile, there is only a slight overlap between the Pt-d states and the C-p states (Fig. 6c). It suggests that there is poorer interaction between Pt and the C support than that between Pt and Ti_3C_2. Therefore, it is easy for Pt NPs ripening and aggregation on carbon support but difficult on Ti_3C_2. Table 1 also tells that the electron transfer happens from C and Ti_3C_2 support to Pt NPs. The transferred electrons (characterized by average net charge) between Pt and the C support are less than those between Pt and Ti_3C_2. It means that Pt NPs contain more electrons in the case of Pt/Ti_3C_2 than in the case of Pt/C. This conclusion is also supported by the XPS results (Fig. 6d), in which Pt $4f_{7/2}$ peak of the Pt/Ti_3C_2 catalyst was shifted to a lower binding energy (71.50 eV) relative to the Pt $4f_{7/2}$ peak of the Pt/C catalyst (71.90 eV). It also suggests that the stronger interaction happens between Ti_3C_2 support and Pt NPs than between C support and Pt NPs. Such a strong interaction between Pt NPs and Ti_3C_2 makes Pt NPs spread out on the Ti_3C_2 support, however the poor interaction between Pt NPs and C only makes Pt NPs pile up on the C support as illustrated in Fig. 6a.

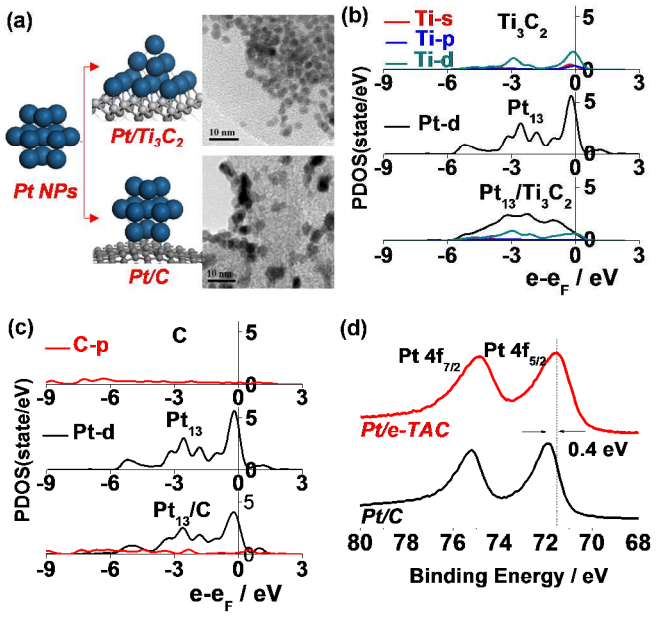

Fig. 6 (a) The optimized most stable structure of Pt_{13} loaded on the Ti_3C_2 and C; The PDOS for (b) Pt/Ti_3C_2 and (c) Pt/C before and after adsorption; (d) Pt 4f XPS spectra of Pt/e-TAC and Pt/C.

On the other hand, by considering the pivotal role of intermediate species O_{ad} and O_2 in ORR, we calculated the adsorption energies (AE) of O_{ad} and O_2 on Pt_{13}/Ti_3C_2, Pt_{13}/C and unsupported Pt_{13}. The results in Table 1 indicate that the adsorption energies (AE) of O_{ad} and O_2 on Pt_{13}/Ti_3C_2 are obviously reduced relative to those on Pt_{13}/C and Pt_{13}. The currently accepted view is that the adsorption of oxygen-containing species on Pt is too strong that it inhibits desorption of the oxygen-containing species and thus

hinders new active sites released for ORR.[24-25] Thus it is conducive to shift the d band centre of catalysts toward lower energies, which leads to the poor adsorption of O_{ad} on the catalysts.[26] The data summarized in Table 1 well explain why the Pt/Ti_3C_2 (Pt/e-TAC) catalyst exhibits the better catalysis for the ORR than Pt/C in addition to keeping excellent stability.

Table 1 Calculated binding energy, d-band centre, average net charge for Pt cluster, and adsorption energy of O species on Pt.

Catalyst	E_{bind} / eV	ε_d / eV	Average net charge[a]	AE / eV	
				O_2	O
Pt_{13}		1.611	0.003	2.070	6.763
Pt_{13}/C	3.762	1.853	-0.027	1.848	4.463
Pt_{13}/Ti_3C_2	5.499	2.462	-0.253	1.359	4.048

[a] Average net charge were calculated according to the Mulliken method.

In summary, we have developed a novel corrosion-resistant and electrically conductive e-TAC support that exhibits a strong interaction with Pt NPs. The Pt/e-TAC catalyst exhibits much higher activity and stability for ORR compared with Pt/C catalyst. The experimental results suggest this significantly enhanced activity and stability of the Pt/e-TAC catalyst is a result of electronic structure changes of Pt NPs upon its strong interaction with the Ti_3C_2 layered structure of the e-TAC support compared to carbon. DFT calculations clarify why the Pt/Ti_3C_2 (Pt/e-TAC) catalyst exhibits the excellent catalysis for the ORR in addition to keeping excellent stability. The use of e-TAC as a catalyst support provides possibilities for developing an active and stable catalyst support aside from carbon supports for an electrochemical device, where catalysts work at a harsh corrosive condition.

This work was financially supported by China National 973 program (2012CB215500 and 2012CB720300), by NSFC of China (Grant Nos. 21176271 and 21276291) and by the Fundamental Research Funds for the Central Universities (CDJZR12228802).

Notes and references

School of Chemistry and Chemical Engineering, Chongqing University, Chongqing, 400044 (China)
Fax: +86 23 65102531
E-mail: liliracial@cqu.edu.cn (Li)
E-mail: zdwei@cqu.edu.cn (Wei)

Electronic Supplementary Information (ESI) available: Experimental Details, Characterization method, XRD and XPS patterns, BET and BJH patterns, SEM-EDS results. See DOI: 10.1039/c000000x/

1. V. M. Vishnyakov, *Vacuum*, 2006, **80**, 1053.
2. M. K. Debe, *Nature*, **2012**, 486, 43.
3. A. A. Topalov, S. Cherevko, A. R. Zeradjanin, J. C. Meier, I. Katsounaros, K. J. J. Mayrhofer, *Chem. Sci.*, 2014, **5**, 631.
4. M. Tada, S. Murata, T. Asakoka, K. Hiroshima, K. Okumura, H. Tanida, T. Uruga, H. Nakanishi, S.-I. Matsumoto, Y. Inada, M. Nomura and Y. Iwasawa, *Angew. Chem. Int. Ed.*, 2007, **46,** 4310.
5. W. Zhang, J. Chen, G. F. Swiegers, Z.-F. Ma and G. G. Wallace, *Nanoscale*, 2010, **2**, 282.
6. D. He, K. Cheng, H. Li, T. Peng, F. Xu, S. Mu and M. Pan, *Langmuir*, 2012, **28**, 3979.
7. K. Lee, J. Zhang, H. Wang and D. P.Wilkonson, *Journal of Applied Electrochemistry*, 2006, **36**, 507.
8. C. Zhang, H. Yu, Y. Li, L. Fu, Y. Gao, W. Song, Z. Shao and B. Yi, *Nanoscale*, 2013, **5**, 6834.
9. Z.-Z. Jiang, Z.-B. Wang, Y.-Y. Chu, D.-M. Gu and G.-P. Yin, *Energy Environ. Sci.*, 2011, **4**, 2558.
10. V. T. H. Ho, K. C. Pillai, H.-L. Chou, C.-J. Pan, J. Rick, W.-N. Su, B.-J. Hwang, J.-F. Lee, H.-S. Sheu and W.-T. Chuang, *Energy Environ. Sci.*, 2011, **4**, 4194.
11. X. H. Wang and Y. C. Zhou, *J. Mater. Sci. Technol.*, 2010, **26**, 385.
12. X. Xie, S. Chen, W. Ding, Y. Nie and Z. Wei, *Chem. Commun.*, 2013, **49**, 10112.
13. M. Naguib, O.Mashtalir, J. Carle, V. Presser, J. Lu, L. Hultman, Y. Gogotsi and M. W. Barsoum, *ACS Nano*, 2012, **6**, 1322.
14. S. Takemoto, M. Hattori, M. Yoshinari, E. Kawada and Y. Oda, *Biomaterials*, 2005, **26**, 829.
15. Y. C. Zhou, X. H. Wang, Z. M. Sun and S. Q. Chen, *J. Mater. Chem.*, 2001, **11**, 2335.
16. F.-J. Lai, H.-L. Chou, L. S. Sarma, D.-Y. Wang, Y.-C. Lin, J.-F. Lee, B.-J. Hwang and C.-C. Chen, *Nanoscale*, 2010, **2**, 573.
17. B. P. Vinayan and S. Ramaprabhu, *Nanoscale*, 2013, **5**, 5109.
18. Y. Lim, S. K. Kim, S.-C. Lee, J. Choi, K. S. Nahm, S. J. Yoo and P. Kim, *Nanoscale*, 2014, **6**, 4038.
19. R. Wang, C. Ruan, D. Kanayeva, K. Lassiter and Y. Li, *Nano Lett.* 2008, **8**, 2625.
20. W. Xu, J. J. Pignatello and W. A. Mitch, *Environ. Sci. Technol.*, 2013, **47**, 7129.
21. C. Wang, M. Chi, D. Li, D. Strmcnik, D. V. D. Vliet, G. Wang, V. Komanicky, K.-L. Chang, A. P. Paulikas, D. Tripkovic, J. Pearson, K. L. More, N. M. Markovic and V. R. Stamenkovic, *J. Am. Chem. Soc.*, 2011, **133**, 14396.
22. C. Koenigsmann, A. C. Santulli, K. Gong, M. B. Vukmirovic, W.-P. Zhou, E. Sutter, S. S. Wong and R. R. Adzic, *J. Am. Chem. Soc.*, 2011, **133**, 9783.
23. D.-H. Lim and J. Wilcox, *J. Phys. Chem. C*, 2011, **115**, 22742.
24. B. Lim, M. Jiang, P. H. C. Camargo, E. C. Cho, J. Tao, X. Lu, Y. Zhu and Y. Xia, *Science*, 2009, **324**, 1302.
25. D. F. Yancey, L. Zhang, R. M. Crooks, G. Henkelman, *Chem. Sci.*, 2012, **3**, 1033.
26. T.-Y. J, N. Pinna, S. J. Yoo, D. Ahn, S, H, Choi, M.-G. Willinger, Y.-H. Cho, K.-S. Lee, H.-Y. Park, S.-H. Yu and Y.-E. Sung, *Nanoscale*, 2012, **4**, 6461.